

Article

Research on Serial VSC-LCC Hybrid HVdc Control Strategy and Filter Design Scheme

Fan Cheng , Lijun Xie  and Zhibing Wang

State Key Laboratory of Operation and Control of Renewable Energy & Storage Systems, China Electrical Power Research Institute, Beijing 100192, China; liju-xie@163.com (L.X.); wangzhibing@epri.sgcc.com.cn (Z.W.)

* Correspondence: chengfan5566@163.com; Tel.: +86-1515-057-2879

Received: 17 December 2019; Accepted: 17 January 2020; Published: 4 May 2020



Abstract: This paper investigated the characteristics of a novel type of hybrid high voltage direct current (HVdc) converter, which is composed by line commutated converter series with voltage source converter. The system and valve level control strategies are introduced, which can provide ac system voltage support. A novel filter design scheme composed by resonant filters for hybrid HVdc are also proposed, which can decrease the capacity of reactive power compensation equipment without deteriorate harmonic characteristics. The ac voltage of HVdc fluctuation level caused by transmitted power variation will be effectively reduced, with the coordination between filter design scheme and converter control. In addition, the influence of ac grid strength is also analyzed by equivalent source internal impedance represented by short circuit ratio (SCR). Finally, the +800 kV/1600 MW hybrid HVdc system connecting two ac grids under different SCR cases are studied, and the PSCAD/EMTDC simulation results have validated the effectiveness for proposed strategy.

Keywords: high voltage direct current (HVdc); line commutated converter (LCC); voltage source converter (VSC); control strategy; filter design; short circuit ratio (SCR)

1. Introduction

The high voltage direct current (HVdc) system has been widely applied in large bulk energy long distance transmission scenarios. At present, the converters for practical HVdc engineering projects adopted can be divided into two types [1], the line commutated converter (LCC) based on Graetz bridge, and the voltage source converter (VSC) based on insulated gate bipolar transistor (IGBT). LCC-HVdc systems have been widely utilized for a long history since the commission of Gotland 100 kV/20 MW in 1930s, and the transmission distance of the ± 1100 kV/12 GW Changji-Guquan Ultra HVdc (UHVdc) engineering project has already surpassed 3000 km [2]. Comparing with LCC-HVdc, the highest capacity and voltage level of VSC-HVdc are ± 500 kV and 3 GW after the future commission of Zhangbei VSC-dc grid in the future [3].

Comprehensively, LCC-HVdc is more competitive in the field of maturity and cost efficiency, while VSC-HVdc has higher operation flexibility and ability for extreme weak system operation. However, LCC-HVdc is lack of the islanded operation and voltage support ability, which requires synchronous sources and large bulk reactive power compensation devices at ac side. Unlike LCC-HVdc, VSC-HVdc can transmit power to islanded system and provide reactive power support without auxiliary devices. Moreover, the LCC-HVdc has commutation failure problem, which threatens the safety operation of ac system dramatically, which do not exist for VSC-HVdc. Therefore, establishing a hybrid HVdc converter combining the advantages of two different converters has aroused extensive attention. In fact, two planning engineering projects: Wudongde ± 800 kV UHVdc [4] and Baihetan ± 800 kV UHVdc [5] have both considered the hybrid scheme composed by LCC and VSC to improve the

operation flexibility. The LCC-VSC hybrid multi-terminal HVdc is also considered as a competitive future plan of Brazilian Amazon region hydro energy transmission [6].

The hybrid LCC-VSC HVdc scheme can also be divided into two types: different converter station combination and single converter with hybrid topology. The former has plenty schemes, including LCC rectifier combining with VSC inverter, which can avoid inverter side commutation failure problem [7], and VSC rectifier combining with LCC inverter, which can transmit power for islanded system such as offshore wind farm [8]. In addition, with the high voltage dc/dc converter application, the multi terminal dc (MTdc) system composed by different voltage level LCC and VSC has also been investigated [8]. In [9], the proposed dc/dc transformer named “DC-Auto” can increase the cost efficiency dramatically. Besides, the operation characteristics of paralleled VSC-HVdc and LCC-HVdc are also studied [10], where VSC operates at the STATCOM mode to provide the reactive power support for LCC. The electromagnetic modelling of LCC-VSC hybrid HVdc is also investigated in [11], with the implementation of improved second order model. However, the station combination hybrid HVdc schemes mentioned above do not fully explore the hybrid scheme advantages at station level, which may not be appropriate for weak ac systems connection scenario.

The latter hybrid scheme is firstly proposed in [11], which series LCC with VSC to construct a hybrid converter station, and the VSC topology adopted two-level voltage source converter (2L-VSC), which can only be used for low voltage situation due to the power losses and serial IGBT dynamic voltage balancing problem. With the birth of an advanced VSC topology: multilevel modular converter (MMC) [12], the serial scheme has raised more attention [13]. The supreme demerits of MMC such as low voltage distortion and high reliability can provide the LCC better performance under ac system fault and disturbance. Meanwhile, LCC can assist the commonly used half bridge (HB) MMC to clear the dc fault by blocking valves without auxiliary devices such as dc circuit breaker or current limiter [14]. In [15], the islanded operation control strategy for serial hybrid scheme for wind energy transmission is also proposed [15], which simplified the wind turbines as 2L-VSC and neglect the ac transmission line influences. Similar hybrid converter based on diode rectifier and VSC is also proposed in [16]. Meanwhile, plenty of researches investigated the hybrid serial converter inverter side application, which revealed that the proposed topology owns better commutation failure prevention and voltage support ability, but the reactive power compensation devices and VSC coordination strategy is not considered. Moreover, the improved serial hybrid scheme with multiple paralleled VSCs with one LCC is likely to be adopted in the future Baihetan ± 800 kV UHVdc project [17], which can also solve the capacity matching problem for LCC and VSC [18,19]. However, the assumption of strong ac system in existing literatures cannot reveal the advantages of grid support ability for serial hybrid HVdc. The change of internal impedance may also influence the harmonic performance of equipped filters and power output characteristics.

It can be concluded that the previous researches mainly considered the serial hybrid HVdc topology dc system operation and fault characteristics, without enough investigation for the ac system interaction with serial hybrid HVdc, especially for the series problems brought by extreme weak ac system connection. For the traditional Cigre benchmark filter scheme adopted in former researches, large bulk reactive power is generated under fundamental frequency, which is not appropriate for the serial hybrid converter with voltage support ability. Thus, the control strategy and novel filter design scheme for serial hybrid HVdc is proposed to support the weak ac system operation. Meanwhile, the change of ac system equivalent impedance also has a marked impact on the ac side electrical component harmonics and voltage fluctuation level, which requires more investigation.

The rest of this paper is organized as follows, the characteristics of serial VSC-LCC hybrid HVdc is investigated, based on the mathematical models of LCC and MMC in the first section. The next section provides the detailed control strategy for hybrid HVdc, containing both the system and valve level. In Section 4, the resonant filter design scheme is compared with the traditional Cigre Benchmark scheme by both the frequency-domain impedance, power loss as well as reactive power compensation capacity. After that, the influence of grid strength is also investigated by equivalent Thevenin circuit

with different short circuit ratio (SCR). In the final section, the simulation cases built in PSCAD/EMTDC platform have proved the effectiveness of proposed strategy and filter design scheme, and the ac voltage fluctuation level under transmitted power changing is reduced dramatically.

2. Hybrid HVdc Topology and Mathematical Model

2.1. Hybrid HVdc Topology

The structure of hybrid HVdc is shown in Figure 1, the upper converter utilizes a LCC, while the lower utilizes HB-MMC-based VSC, because IGBT insulation tolerance is weaker compared with thyristor. For both rectifier and inverter, LCC is series with VSC. It is noteworthy that the figure only showed the positive pole of HVdc, and the negative pole is symmetric.

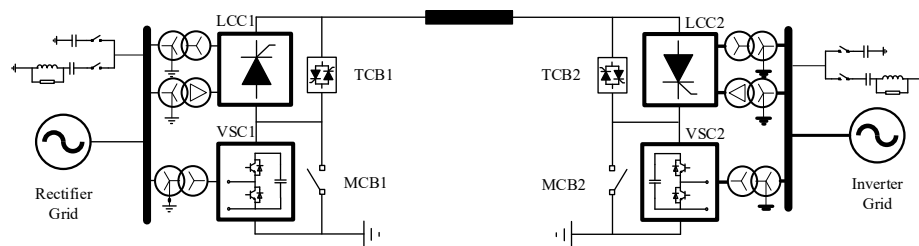


Figure 1. LCC-VSC serial hybrid HVdc structure.

By installing thyristor-based bypass circuit breaker (TCB) switches and mechanical bypass circuit breaker (MCB), there are four typical operation modes for hybrid HVdc as Figure 2 shown. The thyristor bypass switch is composed of antiparallel thyristors, and the status is controlled by the thyristor firing angle.

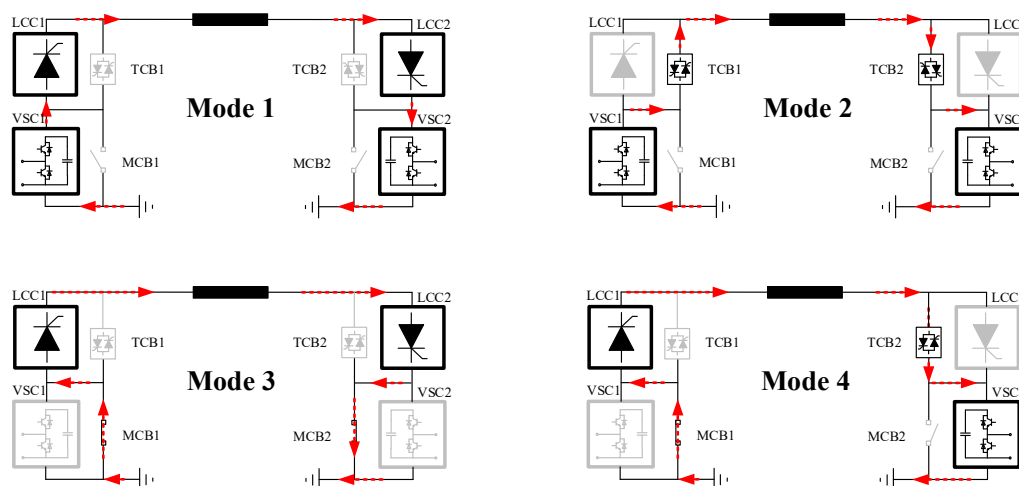


Figure 2. Hybrid high voltage direct current (HVdc) operation modes. Mode 1: Both line commutated converters (LCCs) and voltage source converters (VSCs) are working; mode 2: Only VSCs are working; mode 3: Only LCCs are working; Mode 4: LCC is working on one side, and VSC is working on the other side.

For large-scale renewable energy integration scenario, the active power input fluctuates due to the intermittence and randomness of radiance and wind velocity. If the active power is extremely low (such as lower than 0.1 p.u.), LCC may operate in discontinuous current mode (DCM), which will cause consistent valve overvoltage. Therefore, hybrid HVdc operation modes should be switch the between mode 1 and mode 2, which is realized by the TCB control.

2.2. LCC Mathematical Model

The topology of 12 pulses LCC is shown in the Figure 3, and according to the quasi-steady state formula, LCC rectifier mathematical model can be expressed as:

$$\begin{cases} U_{dcR} = 2\left[1.35U_{acR} \cos \alpha_R - \frac{3}{\pi}X_{r1}I_{dc}\right] \\ P_{acR} \approx P_{dcR} = U_{dcR} \cdot I_{dc} \\ \tan \varphi_R = \frac{1}{2}[\cos \alpha_R + \cos(\alpha_R + \mu_R)] \end{cases}, \quad (1)$$

where U_{dcR} , I_{dc} , P_{dcR} denote the dc voltage, dc current and dc active power, respectively. φ_R , α_R and μ_R denote the rectifier power factor angle, firing angle and commutation angle. X_{r1} is the commutation reactance, and U_{acR} represents the valve side rms L-L value of rectifier ac voltage.

The rectifier commutation angle μ_R can be calculated by:

$$\mu_R = \arccos\left(\cos \alpha_R - \frac{2X_{r1}I_{dc}}{\sqrt{2}U_{acR}}\right) - \alpha_R. \quad (2)$$

Similarly, the inverter mathematical model can be expressed as:

$$\begin{cases} U_{dcI} = 2\left[1.35U_{acI} \cos \gamma_I - \frac{3}{\pi}X_{r2}I_{dc}\right] \\ P_{acI} \approx P_{dcI} = U_{dcI} \cdot I_{dc} \\ \tan \varphi_I = \frac{1}{2}[\cos(\gamma_I + \mu_I) + \cos(\gamma_I)] \end{cases}. \quad (3)$$

Also, the inverter commutation angle μ_I can be calculated by:

$$\mu_I = \arccos\left(\cos \gamma_I - \frac{2X_{r2}I_{dc}}{\sqrt{2}U_{acI}}\right) - \gamma_I, \quad (4)$$

where γ_I denotes the inverter extinction angle which satisfied:

$$\gamma_I = \pi - (\alpha_I + \mu_I) \quad (5)$$

and α_I denotes the inverter firing angle.

According to KVL, rectifier and inverter dc voltage have relationship as:

$$U_{dcR} - U_{dcI} = 2R \cdot I_{dc} \quad (6)$$

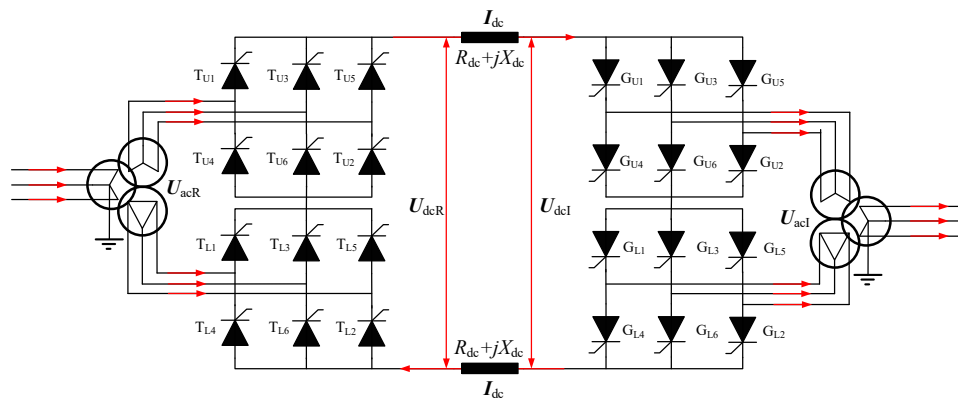


Figure 3. LCC topology.

Normal LCC control strategy applied constant extinction angle (CEA) for inverter and constant current (CC) for rectifier. If the sending grid and receiving grid have enough strength

which can guarantee the ac voltage stable, the operation point of LCC can be easily determined. However, when the LCC is connected with weak grid or islanded grid, the interaction between HVdc and ac grid will be more complicated and new strategy is required. Meanwhile, for islanded grid without synchronous sources, pure LCC-HVdc is impossible to run only if the islanded grid can provide phase angle reference and voltage support.

2.3. VSC Mathematical Model

In most VSC-HVdc projects, HB-MMC topology is used due to its low harmonic, low power losses as well as high reliability comparing with two level VSC. HB-MMC equivalent circuit is shown in the Figure 4, where C_0 represents the half-bridge submodule capacitor and L_0 represents the arm inductor. The current-voltage equation in fundamental frequency based on average switching function can be expressed as:

$$\begin{cases} u_j = \frac{u_{dc}}{2} - L_0 \frac{di_{uj}}{dt} - u_{uj} = -\frac{u_{dc}}{2} + L_0 \frac{di_{lj}}{dt} + u_{lj} \\ i_j = i_{uj} - i_{lj} \\ i_{uj} = S_j \cdot N \cdot C_0 \frac{du_{uj}}{dt} \\ i_{lj} = (1 - S_j) \cdot N \cdot C_0 \frac{du_{lj}}{dt} \end{cases} \quad (7)$$

where j denotes the phase a, b, c, N is the total number of submodules per arm, and S_j is the average switching function for phase j . The active power balance equation can be expressed as:

$$P_{ac} = P_{dc} - P_{loss} - \frac{d}{dt} \left(\frac{3}{2} N C_0 U_{dc}^2 \right) \quad (8)$$

where P_{loss} , P_{ac} , P_{dc} denotes the power loss of MMC, and ac active power output and dc active power input. For MMC connecting with islanded grid, the unbalanced active power will lead to dc voltage fluctuation, and the opposite-end converter station applies constant dc voltage control to determine the operation point.

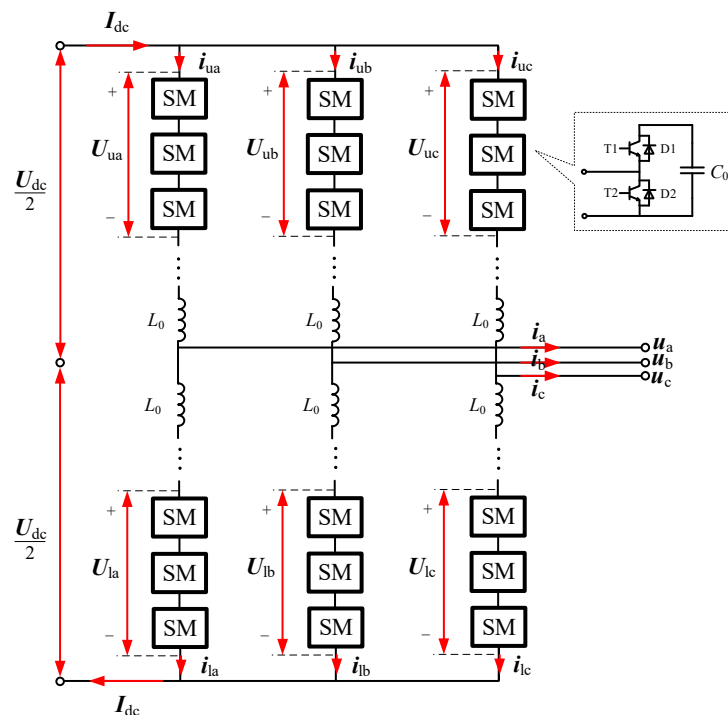


Figure 4. HB-MMC equivalent circuit.

3. Hybrid HVdc Control Strategy

In general, the rectifier side LCC controls the dc current and inverter side LCC controls the extinction angle for pure LCC-HVdc projects. For the serial hybrid HVdc topology, it is noteworthy that LCC rectifier and inverter have already determined the operation point, so only dc voltage of VSCs can be controlled. Therefore, both rectifier and inverter side VSCs can be set as constant dc voltage (Edc control) mode for hybrid HVdc system. Although VSCs can also be operated at active power mode, Edc control is preferred due to the better dc voltage dynamic responses.

3.1. LCC Rectifier and Inverter Control Strategy

Rectifier LCC applies dc current with backup firing angle control, as shown in Figure 5. The dc current order I_{dc_rec} is received from inverter side, and PI controller regulates the firing angle to track I_{dc_rec} for normal condition. The firing angle is limited between 5° and 150° , and the control mode will be automatic changed to constant firing angle if PI controller output has reached the limit value.

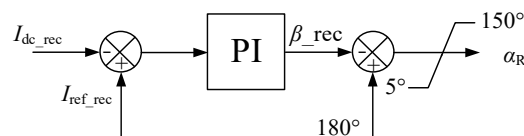


Figure 5. Rectifier LCC control strategy.

LCC inverter control applies constant extinction angle (CEA) with backup constant current (CC) and current margin control (CMC), which is shown in Figure 6. The maximum value selector decides the control mode for LCC inverter. Normally, CEA mode is enabled to decrease the reactive power consumption, and CMC can eliminate the firing angle fluctuation caused by harmonic distortion. I_{dc_rec} is generated by DC current set value and voltage droop current order limiter (VDCOL) minimum value selection mode.

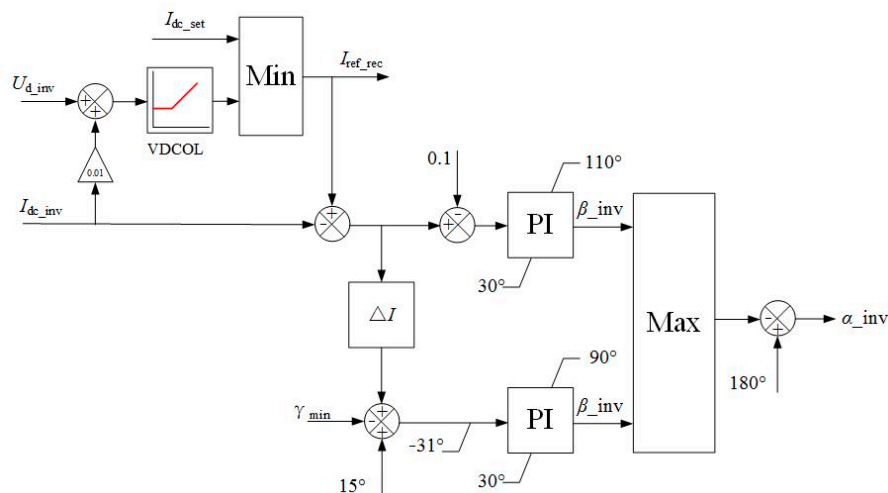


Figure 6. Inverter LCC control strategy.

3.2. VSC Control Strategy

In this paper, VSC topology is selected as HB-MMC, and its control strategy included valve level control and converter level. The former is composed by staircase modulation mode and voltage balancing algorithm, and the latter contained power out loop, current inner loop and circulating current suppression control (CCSC). The VSC converter level control strategy is shown in Figure 7, which applied dc voltage and ac voltage out loop. PLL denotes phase lock loop, which can track

the grid voltage phase angle for coordinate transformation, and the reference rotation axis is set as ac voltage d-axis component. The reactive power control loop contains three PI controller in series, which regulate ac voltage, reactive power output and q-axis current, respectively. The inner current loop adopts feedforward compensation control to enhance the dynamic response, where L denotes the arm inductance. With the implementation of ac voltage outer loop, the VSC reactive power output can be regulated according to the ac voltage level, which is crucial for the safe operation of hybrid serial HVdc. Meanwhile, by changing the number of compensated capacitor banks in Section 4.2, the coordinated strategy can maintain the reactive power exchange between hybrid HVdc and ac system in a reasonable range.

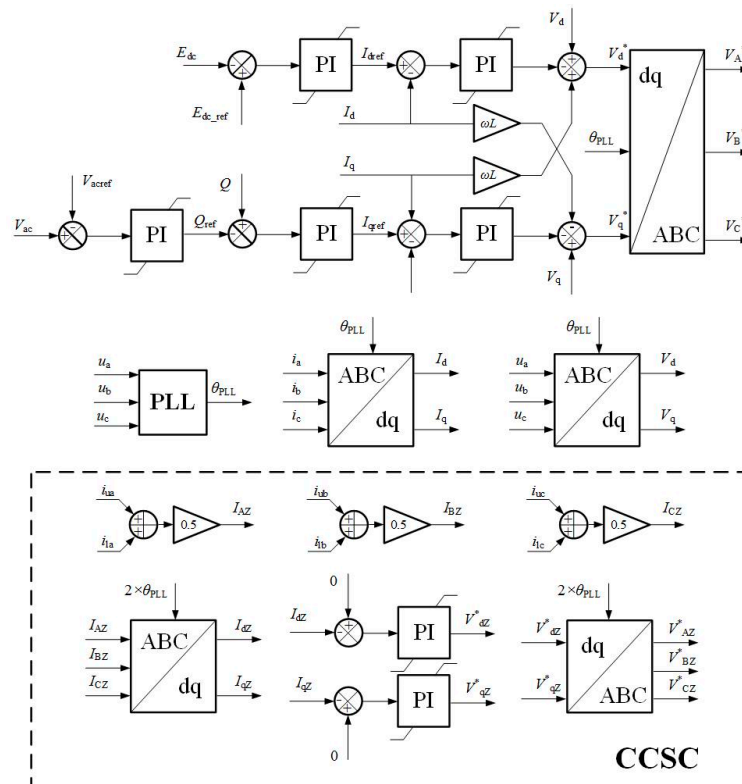


Figure 7. VSC dc and ac voltage control strategy.

4. Filter Design Scheme Based on Resonant Filter and Influences of SCR

4.1. Cigre Benchmark Filter Scheme

Considering the fact that LCC brings 11th, 13th, and other $(12k \pm 1)$ th harmonics into ac grids, passive filters are equipped necessarily for the harmonics elimination. For pure LCC-HVdc, paralleled capacitors with damping branch are applied to eliminate characteristic harmonics and provide reactive power compensation. The typical damping capacitor structure are shown in Figure 8, whose parameters origin from Cigre Benchmark HVdc model at rectifier side.

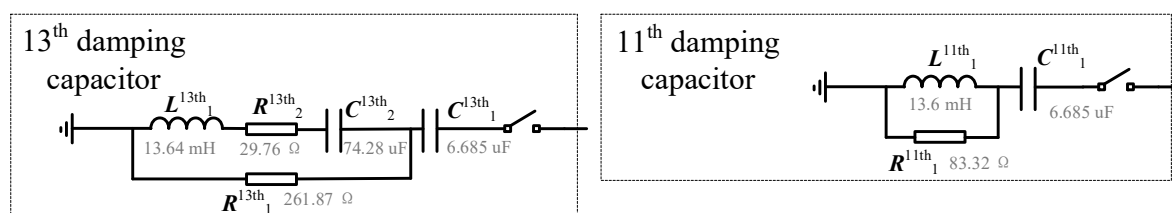


Figure 8. 11th and 13th damping capacitors structure of Cigre Benchmark model.

The 11th and 13th damping capacitor impedance can be written as:

$$Z^{11\text{th}}(s) = \frac{s^2 L_1^{11\text{th}} R_1^{11\text{th}} C_1^{11\text{th}} + s L_1^{11\text{th}} + R_1^{11\text{th}}}{s^2 L_1^{11\text{th}} C_1^{11\text{th}} + s R_1^{11\text{th}} C_1^{11\text{th}}} \quad (9)$$

$$Z^{13\text{th}}(s) = \frac{s^2 L_1^{13\text{th}} R_1^{13\text{th}} C_2^{13\text{th}} + s C_2^{13\text{th}} R_1^{13\text{th}} R_2^{13\text{th}} + R_1^{13\text{th}}}{s^2 L_1^{13\text{th}} C_2^{13\text{th}} + s (R_2^{13\text{th}} + R_1^{13\text{th}}) C_2^{13\text{th}} + 1} + \frac{1}{s C_1^{13\text{th}}} \quad (10)$$

where s denotes the Laplace operator. The Bode diagrams of damping capacitors frequency impedance and phase angle are shown in the Figure 9. It can be seen from the figure that two damping capacitor impedance reaches the minimum value at around 528 Hz and 580 Hz, which is beneficial for 11th and 13th order accompanied harmonics filtering.

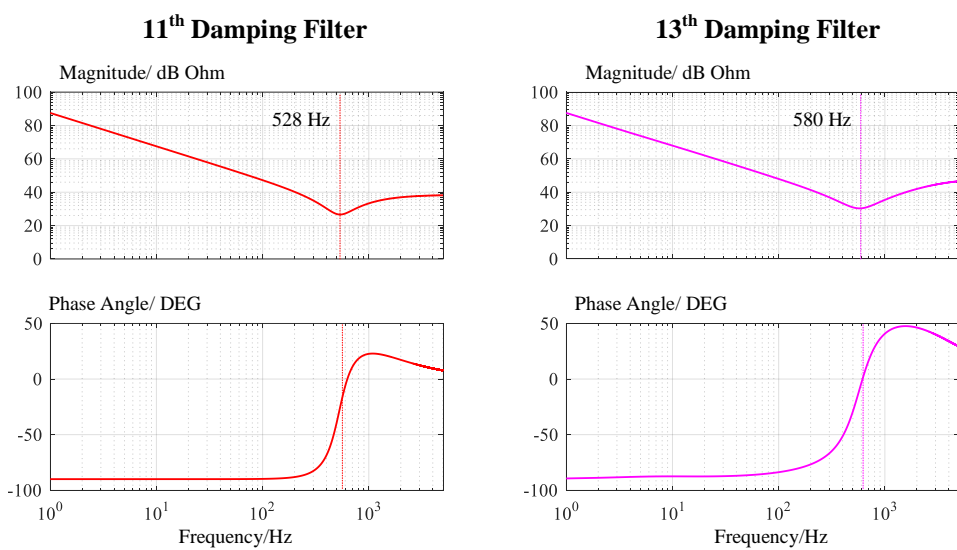


Figure 9. 11th and 13th damping capacitors impedance bode diagrams.

The reactive power compensation $Q^R(s_0)$ and active power loss $P^R(s_0)$ of damping capacitor at fundamental frequency can be calculated through Equation (11). The reactive power compensation for 11th and 13th damping capacitors are around 252 MVar and 234 MVar, and the active power losses are 0.126 MW and 1.469 MW, respectively. If the serial LCC-VSC hybrid HVdc adopts the same type damping capacitor for filtering, it can be deduced that the massive reactive power will be absorbed by VSC during low transmitted power.

$$\begin{cases} P^R(s_0) = \text{Re}(U^2/Z^R(s_0)) \\ Q^R(s_0) = \text{Im}(U^2/Z^R(s_0)) \end{cases} \quad \text{and} \quad s_0 = j2\pi f_0 \quad (11)$$

4.2. Filter Scheme Based on Resonant Filter

To decrease the reactive power exchange between VSC and ac system, a novel filter design scheme based on resonant filter is proposed in this section, and its structure is shown in Figure 10. The scheme can change the reactive power compensation value with switching of capacitor banks, and the characteristic harmonics are filtered by the resonant filters with small reactive power output.

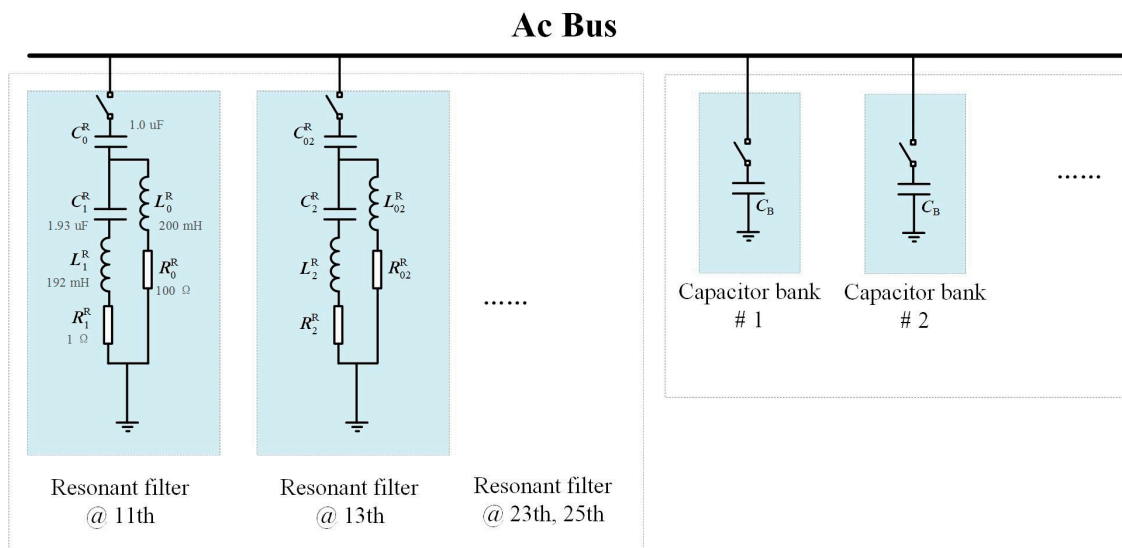


Figure 10. Resonant filter and capacitor structure.

The resonance branch contains the serial capacitor C_1^R and inductor L_1^R , and R_1^R represents the inductor coil resistance. For the resonant filter, the cut-off frequency is decided by C_1^R and L_1^R , while the reactive power output and active power loss can be adjusted by changing the value of C_0^R , L_0^R and R_0^R . Similarly, the resonant filter frequency impedance is expressed as:

$$Z^R(s) = \frac{s^3 L_0^R L_1^R C_1^R + s^2 (R_1^R L_0^R + R_0^R L_1^R) C_1^R + s (R_1^R R_0^R + L_0^R) C_1^R + R_0^R}{s^2 L_1^R C_1^R + s (R_1^R + R_0^R + s L_0^R) C_1^R + 1} + \frac{1}{s C_0^R} \quad (12)$$

The bode diagram of 11th resonant filter with marked parameters is shown in Figure 11, and the impedance magnitude reaches the minimum value at resonant point around 550 Hz. Meanwhile, for 345 kV ac system, the active power consumption and reactive power generation at power frequency 50 Hz are 1.3738 MW and 38.8345 MVar, respectively. Compared with the former 11th damping filter, the reactive power compensation value is much lower, which indicates the LCC characteristic harmonics can be eliminated without massive reactive power generation.

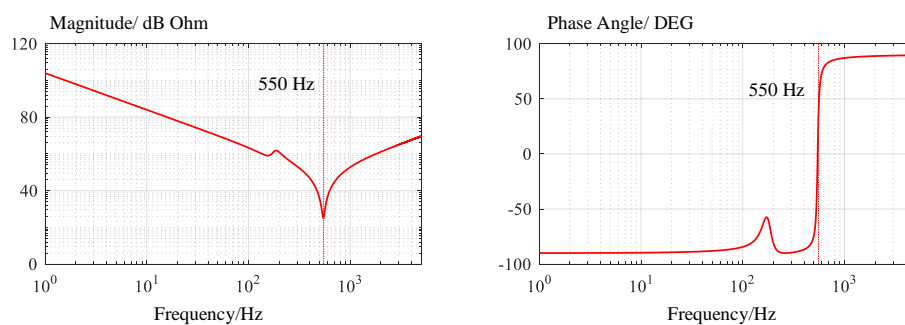


Figure 11. Resonant filter impedance Bode diagrams.

Furthermore, the influence of resonant filter parameters is also investigated, especially for the coil resistance R_1^R . The 3-D surface of frequency impedance for different coil resistance R_1^R is shown in Figure 12a,b, while the active power losses and reactive power compensation are shown in Figure 12c,d. It can be seen from the Figure 12a that with the growth of R_1^R , the cut-off frequency impedance at 550 Hz increases gradually, which means the filtering effect will be worsen. Meanwhile, Figure 12c indicates that the growth of will lead to the slight decrease of total active power loss. Considering the priority of filtering effect, the coil resistance R_1^R should be reduced as much as possible.

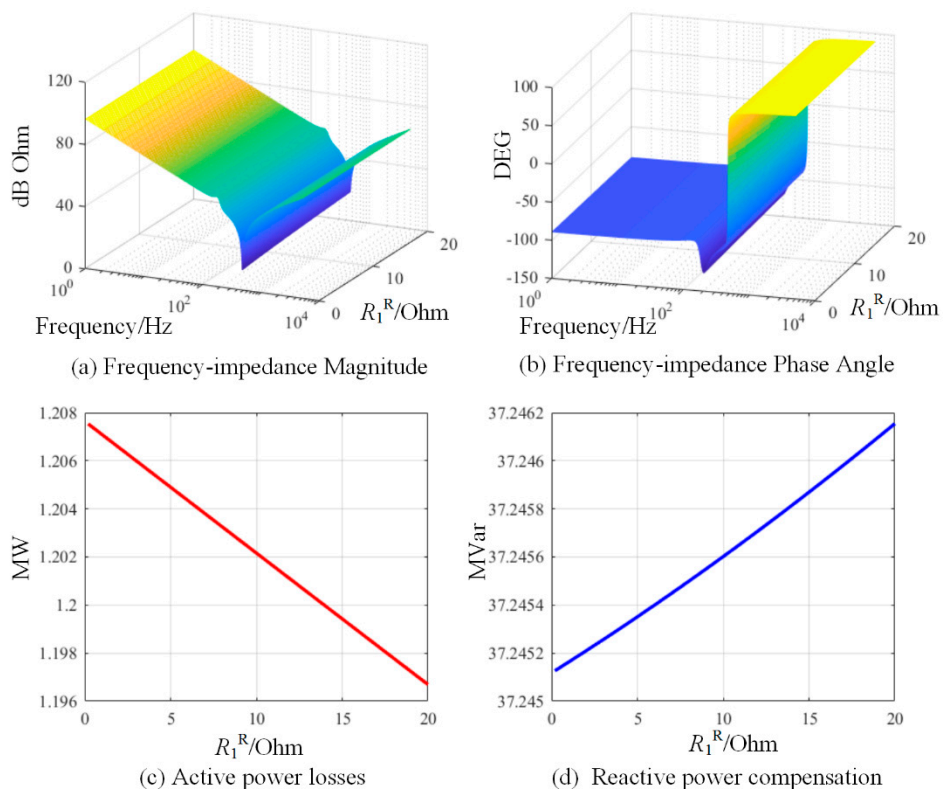


Figure 12. Resonant filter impedance, active power loss and reactive power compensation with different coil resistance.

4.3. Influences of Connected ac System SCR

To indicate the ac system strength level, SCR is normally selected as a critical index. According to the equivalent Thevenin circuit of ac system, the change of SCR would influence the reactive power exchange value and characteristic harmonics filtering effect. Assuming the power factor of LCC is constant, and the accompanied harmonic currents are represented by paralleled current sources with constant magnitude ratio with main component. The LCC and VSC simplified models are shown in Figure 13.

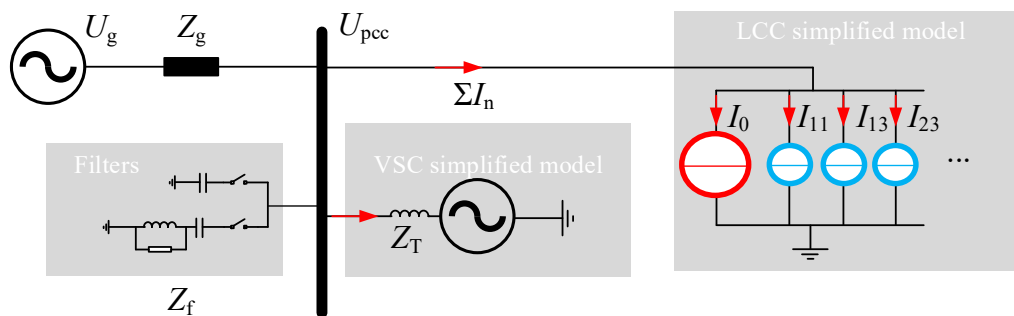


Figure 13. Serial LCC-VSC hybrid HVdc simplified model with ac system connection.

LCC is simplified as a series of paralleled current sources, with the main component I_0 at fundamental frequency, and accompanied harmonic sources I_{11} , I_{13} et al. Serial VSC can be simplified as a voltage source with internal impedance Z_T , which is the sum of transformer leakage inductance and arm reactor. The total impedance of filters and capacitor banks is represented by Z_f , and the

Thevenin equivalent impedance of ac system is Z_g . Therefore, the i -order harmonic currents flow into ac system can be expressed as:

$$I_{gi} = I_i \left[\frac{Z_f(s_i)Z_T(s_i)}{Z_f(s_i)Z_T(s_i) + (Z_f(s_i) + Z_T(s_i))Z_g(s_i)} \right] \quad (13)$$

where s_i represents the Laplace operator at harmonic frequency. Assuming the ac system internal impedance is pure inductance equal with $j\omega L_g$, the growth of SCR means the increase of $Z_g(s_i)$, the harmonic current magnitude would be slightly smaller. However, the growth of Z_g also indicates the voltage fluctuation range caused by active power changing would be wider. Therefore, the influence of SCR should be evaluated in several fields, especial the voltage fluctuation range of different active power transmitted.

5. Simulation

To verify the hybrid serial LCC-VSC HVdc system, a PSCAD/EMTDC simulation case was built, and detailed parameters are listed in Table 1. Both sending grid and receiving grid were simplified as Thevenin equivalent circuit, which was same as the Cigre Benchmark HVdc model. Both sending-end and receiving-end ac systems short circuit capacity were 2500 MVA, and the nominal ac voltages were 345 kV and 230 kV, respectively. The nominal capacity of serial LCC-VSC hybrid HVdc was 1600 MW, which indicates the SCR are 1.5625 for both sending-end and receiving-end ac system. The filter was designed as mentioned above. The whole system start-up process, active power change dynamic and comparison between different SCR ac system are provided in this section, to validate the effectiveness of proposed control strategy and better performance with traditional LCC-HVdc and serial LCC-VSC hybrid HVdc with Cigre Benchmark filter design scheme.

Table 1. Hybrid HVdc System Parameters.

LCC Parameters		VSC Parameters	
Capacity	1000 MW	Capacity	1000 MW
dc voltage	400 kV	dc voltage	400 kV
ac voltage	172.8 kV	ac voltage	220 kV
11th filter	√	No. of cells per arm	258
13th filter	√	Arm inductance	40 mH
PLO Kp	10	Cell capacitor	30 mF
PLO Ki	50	Circuit current	CCSC
Trig mode	equidistant	Maximum current	1.2 p.u.

5.1. Serial Hybrid HVdc Start-Up

The simulation waveforms of hybrid HVdc system start-up are shown in Figure 14a–e, respectively, including ac RMS voltage, dc voltage, dc current at rectifier side, active power and reactive power of LCC, as well as MMC.

After MMC start-up, the dc voltage for both rectifier side and inverter side maintained stable at 400 kV for the preparation of whole system startup. At $t = 3.0$ s, LCC inverter and rectifier trigger signals deblocked, and the dc current reference value I_{dc_ref} increased from 0 p.u. to 1.0 p.u.. From simulation results, the ac grid RMS voltage value fluctuated slightly, which is caused by the start-up process of hybrid HVdc requiring the large bulk of reactive power, and the MMC reactive power output regulated swiftly to maintain the ac grid voltage stable. The Figure 14e reactive power curves revealed that LCC consumed the large bulk of reactive power during start-up, which was provided by MMC.

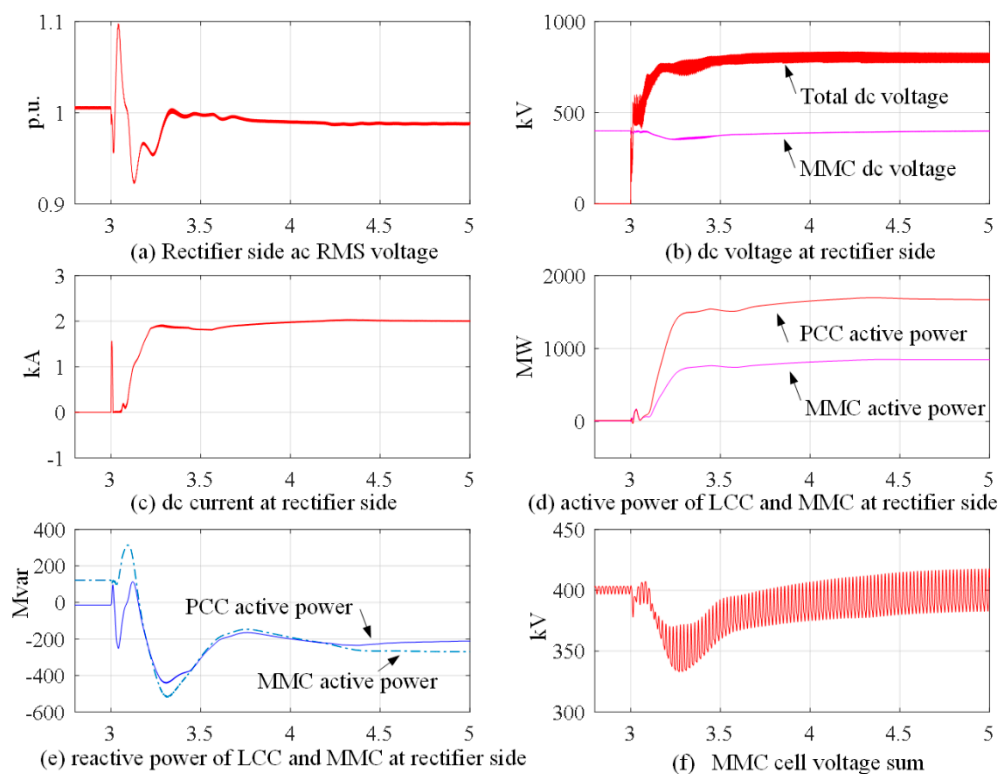


Figure 14. Hybrid HVdc start-up simulation results.

Also, the total submodules voltage of MMC upper arm and lower arm in phase a during start-up is also shown in Figure 14f. The total submodules voltage fluctuated between $\pm 5\%$ p.u., which is acceptable for operation, and the growth of fluctuation was caused by the rise of power output.

5.2. Serial Hybrid HVdc Proposed Scheme Comparison with Cigre Benchmark Filter Scheme

The simulation results of hybrid HVdc system with dc current reference change is shown in Figure 15, where Scheme I denotes the serial hybrid HVdc with Cigre Benchmark filters, and Scheme II represents the serial hybrid HVdc with proposed filter scheme. The connected extreme weak ac systems were the same with 5.1, whose SCR values were both 1.5625. At $t = 9.0$ s, dc current reference value I_{dc_ref} decreased from 1.0 p.u. to 0.85 p.u.. At $t = 11$ s, I_{dc_ref} decreased from 0.85 p.u. to 0.75 p.u.. Finally, at $t = 13$ s, I_{dc_ref} increased from 0.75 p.u. to 0.95 p.u.. The detailed waveforms are shown from Figure 15a–f.

Comparing the ac system rms value curves for both rectifier side and inverter side, scheme I voltage fluctuated in a wider range than scheme II, which indicates the filter scheme proposed could decrease the voltage fluctuation by active power changing better. Meanwhile, Figure 15f provides the detailed curves of reactive power exchange between ac system and hybrid HVdc. It can be directly concluded that the proposed scheme could decrease the reactive power exchange value between ac system and hybrid HVdc. It is noteworthy that the proposed scheme could also provide better damping for dynamic process as Figure 15c shown. Therefore, the comparison verified the proposed scheme had better performance comparing with serial hybrid HVdc with Cigre Benchmark filter scheme.

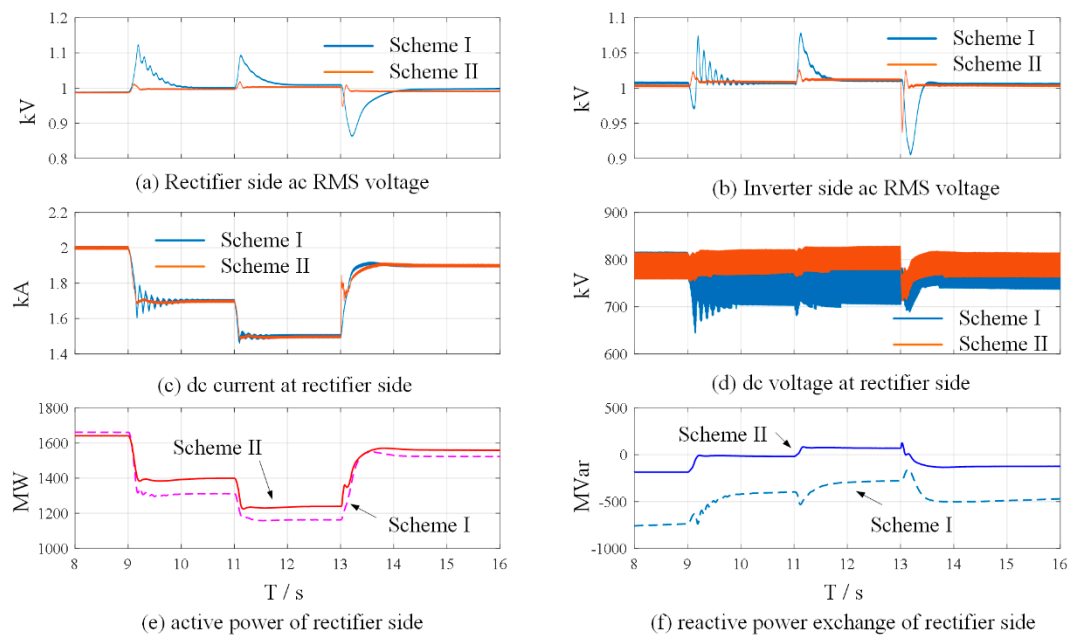


Figure 15. Hybrid HVdc simulation results for dc current reference changing.

5.3. Serial Hybrid HVdc with Different SCR System Connection

From the analysis in Section 4.3, the ac system strength was correlated with the reactive power exchange between ac system and hybrid HVdc converter, as well as harmonic filtering effect. Considering the above system was operated under extreme weak scenario, with SCR lower than 2.0, this section provides the comparison between three equivalent ac systems with different SCR. The three typical SCR values were selected as 1.51625, 3.0, and 5.0, respectively, which can represent the extreme weak ac system, weak ac system, and strong ac system.

The detailed parameters are shown in the Table 2, the rectifier side ac equivalent voltage U_{01} , equivalent impedance magnitude Z_{rec} , impedance phase angle Ph_{rec} , the inverter side ac equivalent voltage U_{02} , equivalent impedance magnitude Z_{inv} and impedance phase angle Ph_{inv} are listed. The FFT results of ac current and voltage for three different scenarios are shown in the Figure 16.

The basic components of ac current and voltage were 1.9524 kA and 140.37 kV, respectively, with the exponential FFT. It can be seen from the figure that the characteristic harmonics at $12k \pm 1$ -order are the main harmonic components. The magnitude of $12k \pm 1$ -order harmonics increased slightly with the growth of SCR, which is consistent with the analysis in Section 4.3. The harmonic components in all three scenarios were pretty low, which can satisfy the requirement of ac system total harmonic distortion (THD).

Table 2. Simplified ac system equivalent Thevenin circuit parameters.

Scenario I Parameters		Scenario II Parameters		Scenario III Parameters	
U_{01}/kV	382.87	U_{01}/kV	363.5	U_{01}/kV	357.33
U_{02}/kV	215	U_{02}/kV	222	U_{02}/kV	225
Z_{rec}/Ohm	47.655	Z_{rec}/Ohm	23.8275	Z_{rec}/Ohm	15.885
Ph_{rec}/Deg	84	Ph_{rec}/Deg	84	Ph_{rec}/Deg	84
Z_{inv}/Ohm	21.2	Z_{inv}/Ohm	10.6	Z_{inv}/Ohm	7.066
Ph_{inv}/Deg	75	Ph_{inv}/Deg	75	Ph_{inv}/Deg	75

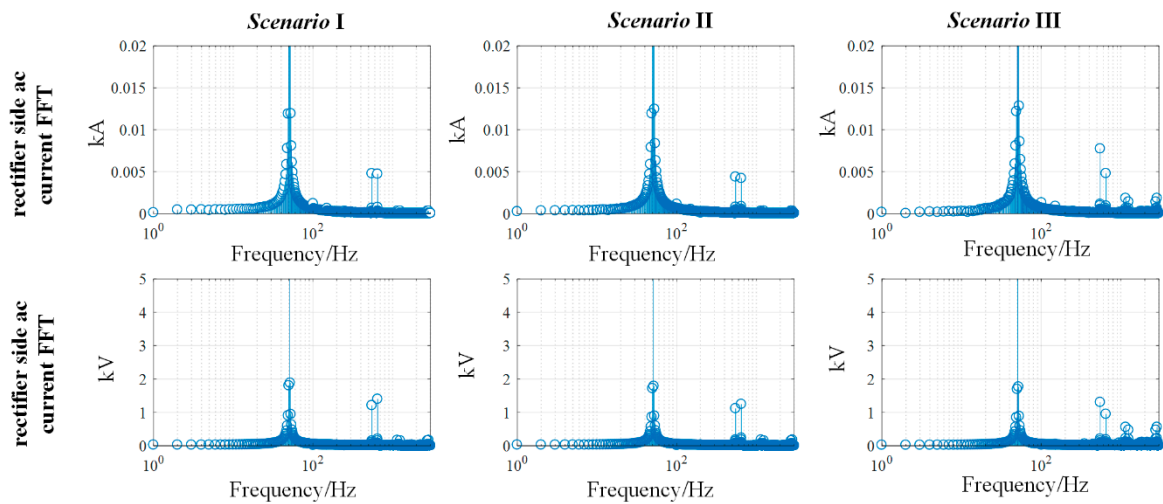


Figure 16. FFT results of ac current and voltage.

The waveforms of different SCR are shown in Figure 17, including the ac RMS voltage and reactive power exchange for both rectifier and inverter side. With the dc current reference value change as Section 5.2, the voltage and reactive power exchange value adjusted. It can be seen from the picture that the growth of SCR decreased the voltage fluctuation range. The fluctuation range for all scenarios were acceptable, which indicates the serial hybrid HVdc under proposed strategy can operate for different ac systems.

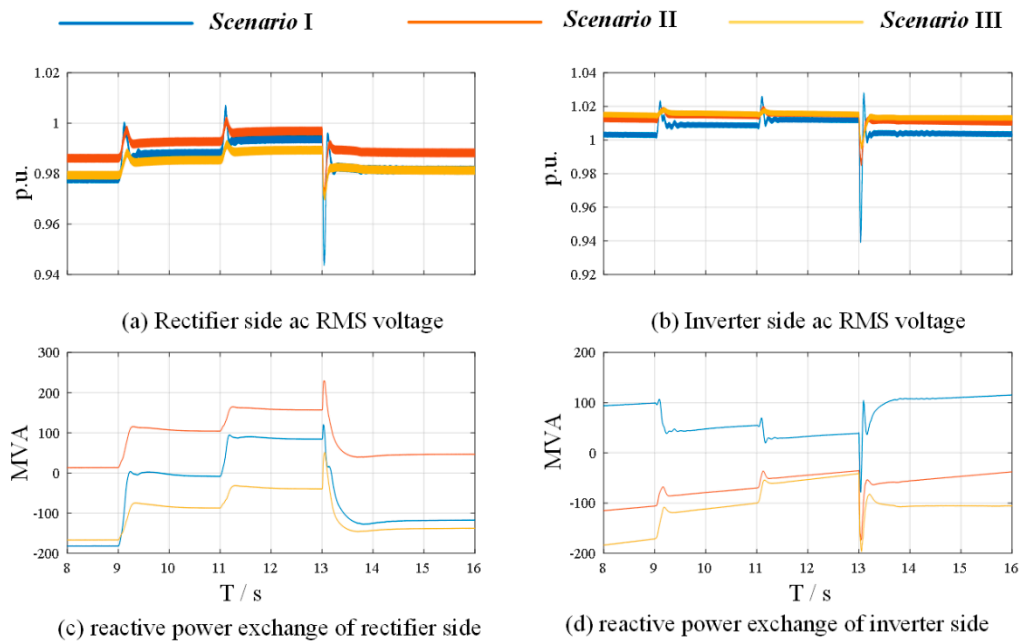


Figure 17. Proposed strategy with different short circuit ratio (SCR).

6. Conclusions

This paper proposed the control strategy and filter design scheme for serial LCC-VSC hybrid HVdc, which can decrease the exchange value of reactive power and provide ac system with voltage support. The characteristics of converters are introduced based on the mathematical model, and the proposed strategy combines the voltage support ability of VSC with LCC operation mode. Foremost, the proposed filter scheme can eliminate the characteristic currents generated by LCC without providing large bulk reactive power, which is suitable for the operation of serial hybrid HVdc.

Meanwhile, the influences of ac system strength is analyzed, which indicates the weaker system brings the ac voltage fluctuation range increase with the active power change. The final PSCAD/EMTDC case of hybrid +800 kV/1600 MW hybrid HVdc system connecting with two weak ac grids simulated the start-up and dc current reference change processes, which validate the effectiveness of proposed strategy. The comparison results with serial hybrid HVdc adopted Cigre Benchmark filter scheme have showed the advantage of proposed control strategy and filter scheme, especially for extreme weak ac system.

Author Contributions: Conceptualization, F.C. and Z.W.; Methodology, F.C.; Validation, F.C. and L.X.; Formal Analysis, F.C.; Investigation, Z.W., L.X. and F.C.; Writing—Review & Editing, F.C.; Supervision, Z.W. All authors have read and agreed to the published version of the manuscript.

Funding: This paper is supported by State Grid Science and Technology Foundation “NY71-19-037: Research on power transmission of large-scale renewable power bases by VSC-LCC hybrid HVdc”.

Conflicts of Interest: The authors declare no conflict of interest.

References

- Li, G.; Liang, J.; Joseph, T.; An, T.; Lu, J.; Szechtman, M.; Andersen, B.R.; Zhuang, Q. Feasibility and Reliability Analysis of LCC DC Grids and LCC/VSC Hybrid DC Grids. *IEEE Access* **2019**, *7*, 22445–22456. [[CrossRef](#)]
- Barnes, M.; Van Hertem, D.; Teeuwssen, S.P.; Callavik, M. HVdc Systems in Smart Grids. *Proc. IEEE* **2017**, *105*, 2082–2098. [[CrossRef](#)]
- Pang, H.; Wei, X. Research on Key Technology and Equipment for Zhangbei 500kV DC Grid. In Proceedings of the 2018 International Power Electronics Conference (IPEC 2018 ECCE Asia), Niigata, Japan, 20–24 May 2018; pp. 2343–2351.
- Rao, H.; Zhou, Y.; Xu, S.; Cai, X.; Cao, W.; Xu, Y.; Ren, C. Key technologies of ultra-high voltage hybrid LCC-VSC MTDC systems. *CSEE J. Power Energy Syst.* **2019**, *5*, 365–373. [[CrossRef](#)]
- Liu, S.; Yu, J.; He, Z.; Liu, Z. Research on Topology and Characteristic of Multi-terminal HVdc Based on VSC and LCC. *Proc. CSEE* **2018**, *38*, 2980–2990.
- Lebre, J.; Portugal, P.; Watanabe, E. Hybrid HVDC (H2VDC) system using current and voltage source converters. *Energies* **2018**, *11*, 1323. [[CrossRef](#)]
- Tang, G.; Xu, Z. A LCC and MMC hybrid HVdc topology with DC line fault clearance capability. *Int. J. Electr. Power Energy Syst.* **2014**, *62*, 419–428. [[CrossRef](#)]
- Zeng, R.; Xu, L.; Yao, L.; Finney, S.J.; Wang, Y. Hybrid HVdc for Integrating Wind Farms with Special Consideration on Commutation Failure. *IEEE Trans. Power Del.* **2016**, *31*, 789–797. [[CrossRef](#)]
- Haleem, N.M.; Rajapakse, A.D.; Gole, A.M.; Fernando, I.T. Investigation of Fault Ride-Through Capability of Hybrid VSC-LCC Multi-Terminal HVdc Transmission Systems. *IEEE Trans. Power Del.* **2019**, *34*, 241–250. [[CrossRef](#)]
- Lin, W. DC–DC Autotransformer with Bidirectional DC Fault Isolating Capability. *IEEE Trans. Power Electron.* **2016**, *31*, 5400–5410. [[CrossRef](#)]
- Xiao, L.; Li, Y.; Xiao, H.; Zhang, Z.; Xu, Z. Electromechanical Transient Modeling of Line Commutated Converter-Modular Multilevel Converter-Based Hybrid Multi-Terminal High Voltage Direct Current Transmission Systems. *Energies* **2018**, *11*, 2102. [[CrossRef](#)]
- Guanglei, L.; Wei, T.; Guanyang, L.; Hongzhao, W.; Yaoyao, W.; Guodong, L. Research on LCC-MTDC and STATCOM technology for wind farms integration. In Proceedings of the 2017 IEEE Conference on Energy Internet and Energy System Integration (EI2), Beijing, China, 26–28 November 2017; pp. 1–6.
- Qahraman, B.; Gole, A. A VSC based series hybrid converter for HVdc transmission. In Proceedings of the Canadian Conference on Electrical and Computer Engineering 2005, Saskatoon, SK, Canada, 1–4 May 2005; pp. 458–461.
- Lesnicar, A.; Marquardt, R. An innovative modular multilevel converter topology suitable for a wide power range. In Proceedings of the IEEE Bologna Power Tech Conference, Bologna, Italy, 23–26 June 2003; pp. 1–5.
- Yang, R.; Xiang, W.; Lin, W.; Wen, J. A hybrid cascaded converter applicable for UHVdc transmission and feeding to load centre. In Proceedings of the 15th IET International Conference on ac and DC Power Transmission (ACDC 2019), Coventry, UK, 5–7 February 2019; pp. 1–6.

16. Guo, C.; Zhao, C.; Peng, M.; Liu, W. A Hybrid HVdc System With DC Fault Ride-Through Capability. *Proc. CSEE* **2015**, *35*, 4345–4353.
17. Lin, W.; Wen, J.; Yao, M.; Wang, S.; Cheng, S.; Li, N. Series VSC-LCC converter with self-commutating and dc fault blocking capabilities. In Proceedings of the 2014 IEEE PES General Meeting Conference & Exposition, National Harbor, MD, USA, 27–31 July 2014; pp. 1–5.
18. Nguyen, T.H.; Lee, D.; Kim, C. A Series-Connected Topology of a Diode Rectifier and a Voltage-Source Converter for an HVdc Transmission System. *IEEE Trans. Power Electron.* **2014**, *29*, 1579–1584. [[CrossRef](#)]
19. Xu, Z.; Wang, S.; Xiao, H. Hybrid high-voltage direct current topology with line commutated converter and modular multilevel converter in series connection suitable for bulk power overhead line transmission. *IET Power Electron.* **2016**, *9*, 2307–2317. [[CrossRef](#)]



© 2020 by the authors. Licensee MDPI, Basel, Switzerland. This article is an open access article distributed under the terms and conditions of the Creative Commons Attribution (CC BY) license (<http://creativecommons.org/licenses/by/4.0/>).